Available online at www.sciencedirect.com
SCIENCE DIRECT®
Journal of Power Sources 119–121 (2003) 226–231
JOURNAL OF POWER SOURCES
www.elsevier.com/locate/jpowsour

MnO_2 (α-, β-, γ-) compounds prepared by hydrothermal-electrochemical synthesis: characterization, morphology, and lithium insertion behavior

Laurie I. Hill*, Alain Verbaere, Dominique Guyomard

Institut des Matériaux Jean Rouxel, 2 rue de la Houssinière, BP32229, 44322 Nantes, France

Abstract

The hydrothermal-electrochemical synthesis route has been used to prepare a variety of MnO_2 compounds with the α, β and γ structure types as well as intimate mixtures of these structure types. The γ-MnO_2 compounds can be synthesized with varying amounts of pyrolusite intergrowth, and low occurrence of microtwinning defects. The influence of the synthesis parameters (temperature, pH, applied current density, composition of the synthesis solution) on the type of structure obtained are discussed. The morphology of some of the compounds obtained is presented. A lithium insertion study compares the behavior of α- and γ-MnO_2. The α-MnO_2 shows a very stable capacity of 145 mAh/g at a discharge rate of C/10.
© 2003 Elsevier Science B.V. All rights reserved.

Keywords: Manganese dioxides; Hydrothermal-electrochemical synthesis; Morphology; Lithium insertion properties

1. Introduction

MnO_2 compounds are among the many materials currently under investigation as positive electrodes for lithium batteries. Compared to vanadium-based oxides, manganese dioxides are advantageous because of their lower cost, lower toxicity and higher average voltage.

α- and γ-MnO_2 compounds are favorable candidates with one-dimensional tunnel structures. The structure of α-MnO_2 (Fig. 1a) is made up of double chains of edge-sharing octahedra which then share corners to form 2×2 and 1×1 channels, the former of which are of suitable size for the insertion/extraction of Li^+. Naturally occurring α-MnO_2 is found with large cations occupying the channels, such as K^+ (cryptomelane) or Ba^{2+} (hollandite) [1–3]. For battery applications, it is desirable to eliminate these large cations (which may impede the diffusion of Li^+), and thus a number of preparations have been used to synthesize α-MnO_2 with only Li^+ or H_3O^+ in the channels. This can be achieved by ion-exchange [4,5] or by direct chemical synthesis [6,7].

The structure of γ-MnO_2 (Fig. 1b) is more complex than that of α-MnO_2. Following the work of De Wolff [8], the structure of γ-MnO_2 is considered to be a random intergrowth of the ramsdellite (2×1 channels) and pyrolusite (1×1 channels) structures, where the amount of pyrolusite intergrowth is denoted as P_r (in percent). To better explain the wide variety of powder X-ray diffraction patterns obtained for γ-MnO_2 compounds, Chabre and Pannetier [9] proposed another defect, microtwinning, the relative amount of which will be denoted here as Mt (in percent) [10]. The relative amounts of pyrolusite intergrowth and microtwinning defects can be determined from the X-ray powder diagrams by measuring the position of the (1 1 0) line and the difference between the positions of the (0 2 1) and (2 4 0) lines of ramsdellite, and comparing these values to those obtained for calculated X-ray diagrams [11]. For industrial applications, γ-MnO_2 is typically synthesized by electrochemical oxidation of acidic $MnSO_4$ solutions. These materials (EMDs) are characterized by a $P_r \approx 50$ and $Mt \geq 50$ [9].

Given that the larger tunnels of the ramsdellite structure are better able to accommodate lithium insertion, and microtwinning defects may inhibit the mobility of the Li^+ ions through the structure, it is anticipated that materials with lower values of P_r and Mt will show superior lithium insertion properties.

The hydrothermal-electrochemical synthesis technique has recently been used for the preparation of a number of transition metal oxides including $LiCoO_2$ and $LiNiO_2$ [12,13]. We have chosen to explore this method with the goal of synthesizing new or modified manganese dioxides and γ-MnO_2 materials approaching the ramsdellite limit.

* Corresponding author.

0378-7753/03/$ – see front matter © 2003 Elsevier Science B.V. All rights reserved.
doi:10.1016/S0378-7753(03)00238-6

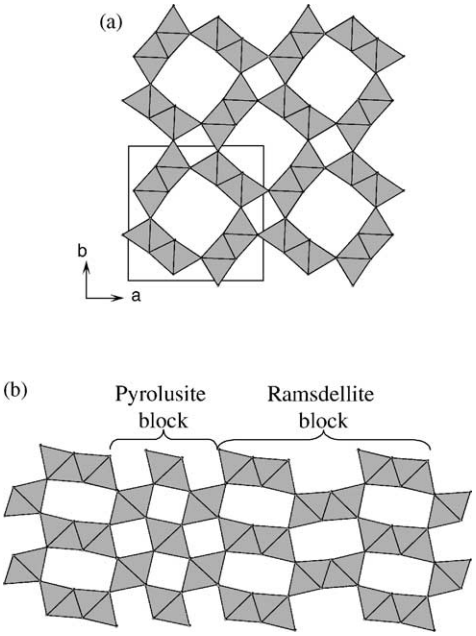

Fig. 1. Structures of (a) α-MnO_2, and (b) γ-MnO_2 showing the intergrowth of ramsdellite and pyrolusite structures.

2. Experimental

2.1. Synthesis

The materials synthesized here were prepared by oxidation of an acidic $MnSO_4$ (0.3 M) or $MnSO_4/Li_2SO_4$ (0.3 M/1.5 M) solution in a stainless steel autoclave with a Teflon liner. The autoclave was equipped with outlets for connection of the working (Au plate, 3.5×4.2 cm^2), counter (two vitreous carbon plates, 3.4×4 cm^2 each) and reference (anodized Ag wire) electrodes to an external potentiostat (MacPile, Biologic, Claix, France). The acidity of the solution was adjusted by the addition of concentrated H_2SO_4. The pH of the solution thus ranged from −0.5 (calculated based on amount of H_2SO_4 added) to 2 ($MnSO_4$ solutions) or 7.7 ($MnSO_4/Li_2SO_4$ solutions). The synthesis temperature was in the range 80–180 °C, and the range of applied current densities was 0.36–36 mA/cm^2. Electrolysis was carried out long enough to obtain 500–600 mg MnO_2. After the synthesis, the product was thoroughly rinsed with distilled water, dried for 2 h at 50–75 °C and removed from the electrode. Before battery studies, the samples were annealed in air at 250 °C for 16 h to decrease the water content.

2.2. Characterization

Analysis of the materials obtained was carried out using X-ray powder diffraction (Cu Kα radiation), thermogravimetric analysis/differential scanning calorimetry (TGA/DSC), atomic absorption spectroscopy/inductively coupled plasma (AAS/ICP) analysis, and redox titration (with a relative precision of ca. 1%). The morphology of the deposits was observed using a scanning electron microscope.

2.3. Lithium insertion studies

Battery studies were conducted using laboratory Swagelok™ cells consisting of a composite cathode (70 wt.% active material, 20 wt.% carbon black, 10 wt.% PVDF binder), a separator soaked in electrolyte (1 M $LiPF_6$ in 2:1 ethylene carbonate (EC):dimethyl carbonate (DMC)) and a lithium metal anode. Cycling was performed in potentiodynamic (first three cycles, 20 mV/h) and galvanostatic (following cycles, C/10 rate) modes in the voltage range 2–4 V using a MacPile system (Biologic, Claix, France).

3. Results and discussion

3.1. Synthesis

The formation of MnO_2 at the electrode occurs according to Reaction 1:

$$Mn^{2+} + 2H_2O \rightarrow MnO_2 + 4H^+ + 2e^- \quad (1)$$

For syntheses carried out at current densities less than 36 mA/cm^2 (0.36, 1.8 or 9.0 mA/cm^2), and pH ≥ 0, the Faradaic yield was near 100%, indicating that all the current was consumed for the formation of MnO_2. In the case of an applied current density of 36 mA/cm^2, the yield was significantly lower (<50%). In this case, the measured voltage during the synthesis was greater than 1.5 V, thus superior to the voltage corresponding to the oxidation of water. For experiments carried out at pH < 0, the yield of MnO_2 was also significantly lower than 100% (∼60%). The measured voltage was, however, inferior to that corresponding to the oxidation of water, indicating that this side reaction was not responsible for the decreased yield. Inspection of the solution after electrolysis showed a bright rose color, characteristic of MnO_4^-. One can thus conclude that it is the simultaneous formation of MnO_4^- which is responsible for the decreased yield. This analysis is in agreement with information contained in the Pourbaix diagrams [14].

3.2. X-ray diffraction and characterization

In using the hydrothermal-electrochemical synthesis technique, a variety of MnO_2 materials with α-, β-, γ- or α·γ-structures have been synthesized in one step [15,16]. X-ray powder diagrams of representative compounds are shown in Fig. 2. The β-MnO_2 compounds (independent of synthesis conditions) display very sharp, intense peaks as seen in the top pattern. The α-MnO_2 in Fig. 2 (bottom pattern) also shows sharp, intense peaks, though other α-MnO_2 compounds prepared in this study showed much broader, less intense peaks. The γ-MnO_2 compounds show a relatively high degree of crystallization (sharper, more intense peaks, more peaks visible) in comparison with γ-MnO_2 compounds synthesized by more traditional methods (broad, low intensity peaks, few peaks visible) [9]. The relative amounts of

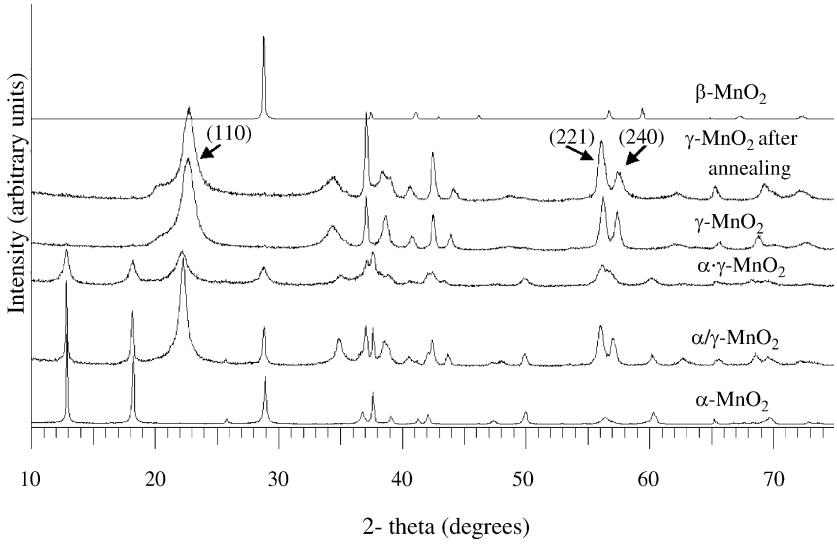

Fig. 2. X-ray diffraction patterns of some of the materials obtained in this study.

pyrolusite intergrowth, P_r, and microtwinning defects, Mt, can be determined based on the positions of the (1 1 0), (2 2 1) and (2 4 0) peaks, highlighted in the figure. Briefly, a shift to higher angle of the (1 1 0) line corresponds to an increase in P_r, while a narrowing of the distance between the (2 2 1) and (2 4 0) lines corresponds to an increase in Mt [9,10,17]. The γ-MnO_2 compounds synthesized here are characterized by P_r values in the range $25 < P_r < 70$ and Mt values near 20. Heat treatment of γ-MnO_2 compounds usually results in an increase in P_r and an accompanying decrease in Mt [9]. However, a majority of the materials obtained here exhibit the unusual property of maintaining a nearly constant P_r, along with the usual decrease in Mt, upon heat treatment. An example is shown in the figure: qualitatively, the position of the (1 1 0) peak remains the same (indicating a constant P_r), while there is a slight increase in the distance between the (2 2 1) and (2 4 0) peaks (indicating a decrease in Mt).

In addition to the pure phases, mixtures were also obtained. Shown in Fig. 2 are two materials characterized as mixtures of α- and γ-MnO_2. The first, noted as α/γ-MnO_2, displays narrow peaks corresponding to each structure. The second, noted as α·γ-MnO_2, displays much broader peaks, an observation which suggests a more intimate mixture (smaller domains) of the two phases and possibly some intergrowth (analogous to the case of γ-MnO_2). Further studies using electron diffraction have confirmed that a large portion of the crystals in the latter sample (α·γ-MnO_2) display a structural interconnectivity between the two phases [16], similar to that reported by Johnson et al. [18], while the former (α/γ-MnO_2) consists of phase separated crystals.

The influence of the synthesis parameters (temperature, pH, applied current density) on the type of structure obtained is summarized in Fig. 3. It is noted that the presence of Li^+ in the solution only had an effect on the structure obtained at very low pH (−0.5, 92 °C) or low temperature (80 °C, pH = 0). For a current density of 0.36 mA/cm^2, higher temperatures and higher pH favor the formation of denser structures. Starting with the lower left corner of the figure, α-MnO_2 is formed in the presence of Li^+, while mixtures of α- and γ-MnO_2 (α/γ or α·γ) are formed in the absence of Li^+. Upon increasing the temperature or the pH of the solution, a wide region of stability for the formation of γ-MnO_2 is found, followed by mixtures of γ- and β-MnO_2. Continuing to increase the temperature leads to the synthesis of well-crystallized β-MnO_2. The formation of β-MnO_2 at higher temperatures in not surprising, given that this structure is more thermodynamically stable than γ-MnO_2. The appearance of α-MnO_2 at low pH may indicate a template or structure directing effect by H_3O^+ (or Li^+ in the case of $MnSO_4/Li_2SO_4$ solutions).

The γ-MnO_2 compounds exhibiting the lowest P_r and Mt values were obtained at pH = 0 and 92 °C in the absence of Li^+. It was thus under these conditions that a study of the influence of the applied current density was undertaken. As seen in the figure, increasing the current density initially leads to the formation of α-MnO_2 (1.8 mA/cm^2) but then leads to the formation of γ-MnO_2 at higher current densities (9.0 and 36 mA/cm^2). It is noted that these γ-MnO_2 compounds show significantly decreased crystallinity by powder X-ray diffraction and significantly increased levels of microtwinning defects (resembling traditional EMDs). At first glance, it is surprising to see the appearance of α-MnO_2 between two regions of γ-MnO_2 formation. This may be attributed to a decrease in the local pH at the electrode, thus mirroring the results obtained at 0.36 mA/cm^2. Continuing this line of reasoning, the results at 9.0 and 36 mA/cm^2 suggest that γ-MnO_2 would again be obtained (at 0.36 mA/cm^2) on further lowering the pH beyond that used in the course of this study.

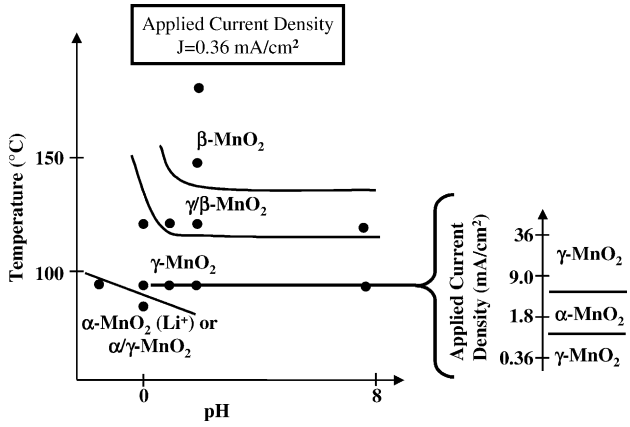

Fig. 3. Phase diagram illustrating the type of structure obtained as a function of temperature and pH (applied current density, J, of 0.36 mA/cm^2) for materials synthesized (circles) using the hydrothermal-electrochemical method. Also presented is the influence of the applied current density, at 92 °C and pH = 0, on the type of structure obtained.

3.3. Physico-chemical characterization

The structural water content (corresponding to a gradual mass loss between 100 °C and 450–500 °C before the decomposition to Mn_2O_3 at about 550 °C), n in $MnO_2{\cdot}nH_2O$, of the materials synthesized in this study was determined by thermogravimetric analysis. The results showed that for the γ-MnO_2 materials, n ranged from 0.05 to 0.1 as synthesized, and from 0.02 to 0.05 after annealing at 250 °C for 16 h. For α-MnO_2 (and α/γ phases), the water content was higher, n as high as 0.2, owing to the larger 2 × 2 tunnels of the α-MnO_2 structure, but very little water remained after annealing ($n < 0.02$).

AAS/ICP analysis was carried out for those samples synthesized from $MnSO_4/Li_2SO_4$ solutions. The γ-MnO_2 compounds showed no incorporation of Li (<0.01 Li/Mn), while the α-MnO_2 materials contained only a small amount of lithium (≤0.05 Li/Mn). Redox titrations were performed to determine the average oxidation state of Mn. The results indicated that Mn is in the 4+ oxidation state for all β-MnO_2. For the α- and γ-MnO_2 synthesized at 0.36 mA/cm^2 the average oxidation state ranged from 3.97 to 4.00+. For α-MnO_2 prepared at 9.0 mA/cm^2, the Mn oxidation state was determined to be +3.96.

3.4. Morphology

A complete SEM study of the deposited MnO_2 materials was undertaken and showed that the morphology and particle size can be controlled by changing the synthesis parameters [19]. A brief summary of the α- and γ-MnO_2 morphologies obtained for an applied current density of 0.36 mA/cm^2 will be presented here. In the case of α-MnO_2, two morphologies were observed with very different particle sizes. The first, shown in Fig. 4a (corresponding to the XRD pattern in Fig. 2) and obtained at pH = −0.5 and 92 °C from $MnSO_4/Li_2SO_4$ solution, can be described as particles in the shape of obelisks approximately 1 μm across. The second morphology, shown in Fig. 4b and obtained at pH = 0 and 80 °C from $MnSO_4/Li_2SO_4$ solution, consists of bundles of very small fibers (∼15–25 nm in diameter) which are arranged in star-like formations.

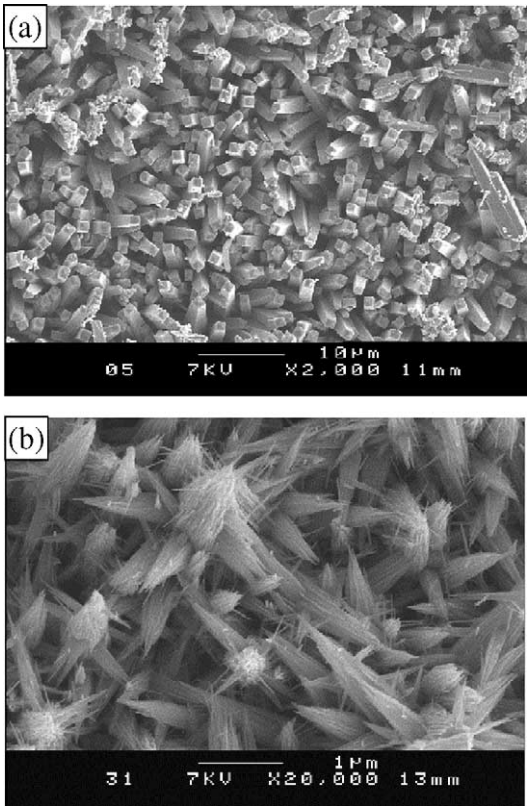

Fig. 4. SEM photographs of α-MnO_2 samples prepared under different conditions: (a) 92 °C, pH = −0.5, $MnSO_4/Li_2SO_4$ solution, and (b) 80 °C, pH = 0, $MnSO_4/Li_2SO_4$ solution.

A number of different morphologies were also obtained for γ-MnO_2, which are independent of the structural parameters (P_r, Mt) of the material. Three of these morphologies are shown in Fig. 5. Fig. 5a shows the morphology of a γ-MnO_2 with structural parameters (43,20) prepared at pH = 0 and 92 °C from $MnSO_4/Li_2SO_4$ solution. Here the surface of the deposit consists of small needle-like fibers approximately 100–200 nm across. For a γ-MnO_2 with structural parameters (49,25) prepared at pH = 1 and 92 °C from $MnSO_4$ solution, shown in Fig. 5b, the observed morphology is that of rod-like fibers with rounded tops approximately 200 nm in diameter. Finally, presented in Fig. 5c is the morphology of a γ-MnO_2 with structural parameters (41,21) prepared at pH = 7.7 and 92 °C from $MnSO_4/Li_2SO_4$ solution. This compound appears as fibrous bundles (up to 0.5 μm in diameter, largely parallel to the surface of the electrode, which are then made up of smaller needle-like fibers about 30–50 nm in diameter. The arrangement of the fibrous bundles results in shapes that resemble evergreen-tree cutouts. It is important to note that the compounds shown in Fig. 5a and c are characterized by

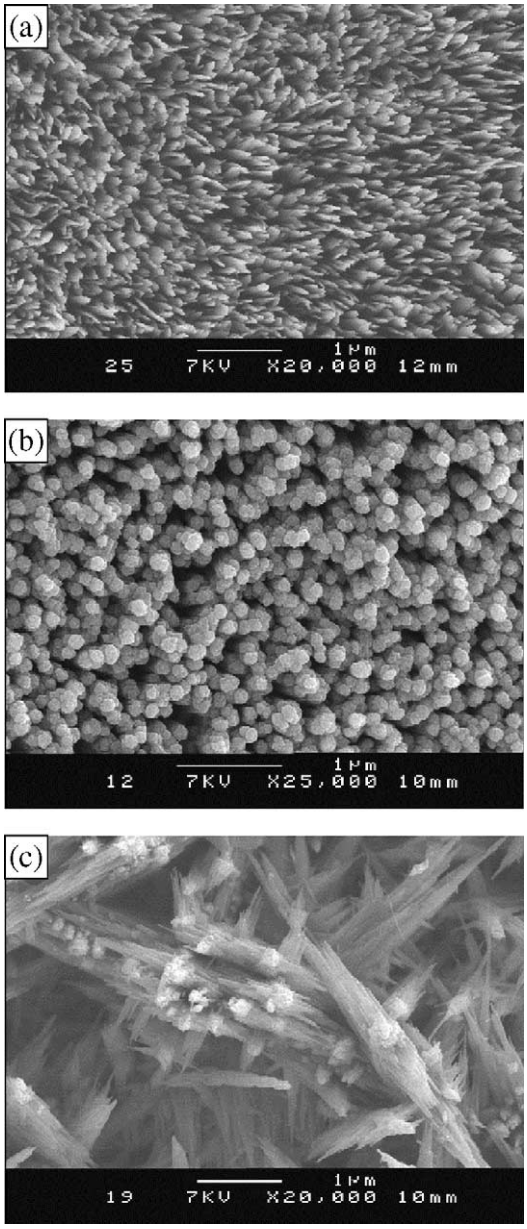

Fig. 5. SEM photographs of γ-MnO_2 samples prepared under different conditions (structural parameters (P_r, Mt) given in parentheses): (a) 92 °C, pH = 0, $MnSO_4/Li_2SO_4$ solution (43,20); (b) 92 °C, pH = 1, $MnSO_4$ solution (49,25); (c) 92 °C, pH = 7.7, $MnSO_4/Li_2SO_4$ solution (41,21).

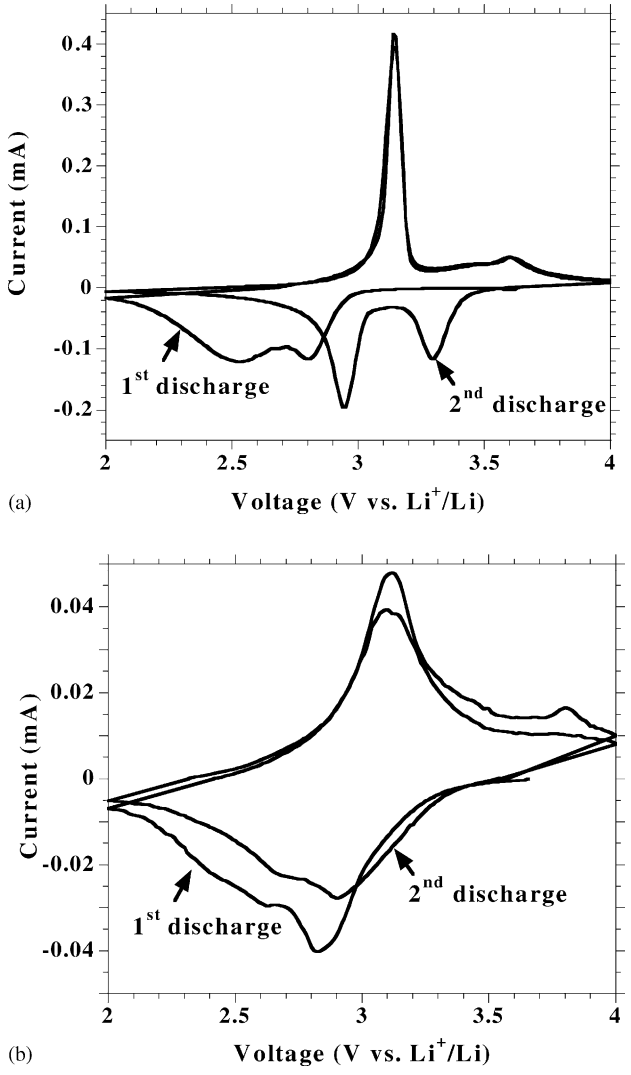

Fig. 6. Current vs. voltage curves of the first two cycles in potentiodynamic mode (20 mV/h) for two compounds synthesized by the hydrothermal-electrochemical method: (a) γ-MnO_2 with structural parameters (45,14), and (b) α-MnO_2.

roughly the same structural parameters, but display quite different morphologies. It can thus be concluded that it is the synthesis parameters which control the morphology.

3.5. Lithium insertion behavior

Fig. 6 shows the current versus voltage curves for a γ-MnO_2 (P_r = 45, Mt = 14) (a) and an α-MnO_2 (b) for the first two cycles in potentiodynamic mode (20 mV/h). For γ-MnO_2, the first two discharge curves are significantly different, marking an irreversible transformation during the first discharge. On the second discharge, the Li^+ insertion occurs in two distinct steps at 3.3 and 2.95 V versus Li^+/Li. This is consistent with previously published results [10,20]. The initial capacity for this compound was 282 mAh/g with a reversible capacity of 231 mAh/g for the second discharge, comparable with the capacity for a similar compound previously studied in our group [21].

Unlike the curves for γ-MnO_2, the first two discharge curves for α-MnO_2 have approximately the same shape, indicating no transformation takes place. The Li^+ insertion appears to occur in several non-resolved steps during discharge and one broad step during charge, contrary to what was observed by Rossouw et al. [3] where two well-resolved steps were observed during both discharge and charge. The initial discharge capacity was 243 mAh/g, with a reversible capacity of 181 mAh/g on the second discharge. These results are in accordance with other reported α-MnO_2's [22,23].

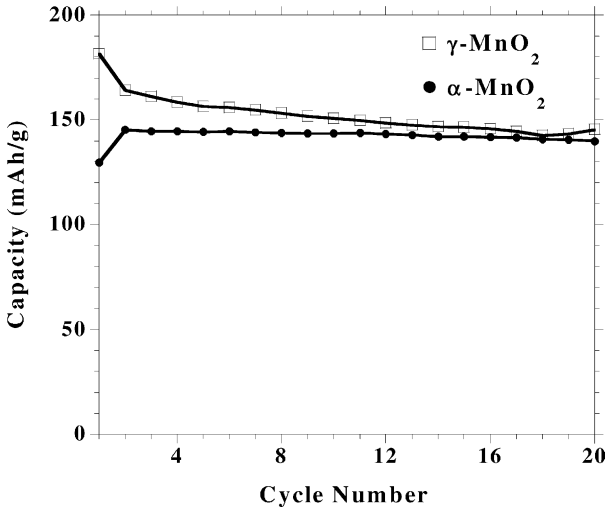

Fig. 7. Capacity as a function of cycle number in galvanostatic cycling mode (C/10 rate) for the two compounds presented in Fig. 5.

Fig. 7 shows the cycled capacity in galvanostatic mode (C/10) for the two materials presented in Fig. 6. The γ-MnO_2 shows a good capacity which slowly fades to a value of ∼150 mAh/g after 20 cycles. The α-MnO_2 compound shows a slightly lower capacity (∼145 mAh/g) but exhibits very stable cycling properties.

4. Conclusion

It has been illustrated that the hydrothermal-electrochemical method can be used to synthesize a variety of MnO_2 compounds of the α, β, and γ structure types. It is also possible to obtain intimate mixtures of these structures, such as interconnected α·γ-MnO_2. By adjusting the experimental parameters such as temperature, pH, presence of Li_2SO_4 in the solution, or the applied current density one can control the type of structure obtained. γ-MnO_2 can thus be prepared over a wide range of P_r values (25–70) and with relatively low levels of microtwinning defects (∼20). An SEM study has shown that the morphology can also be controlled by adjusting the synthesis parameters. The morphology of γ-MnO_2 is independent of the structural parameters of the material. A lithium insertion study has revealed that both γ- and α-MnO_2 compounds synthesized by this method exhibit good capacities, the α-MnO_2 displaying very stable cycling behavior.

References

[1] A. Byström, A.M. Byström, Acta Crystallogr. 3 (1950) 146.
[2] A. Byström, A.M. Byström, Acta Crystallogr. 4 (1951) 469.
[3] M.H. Rossouw, D.C. Liles, M.M. Thackeray, Mater. Res. Bull. 27 (1992) 221.
[4] M. Tsuji, M. Abe, Solvent Extr. Ion Exch. 2 (1984) 253.
[5] C.S. Johnson, D.W. Dees, M.F. Mansuetto, M.M. Thackeray, D.R. Vissers, D. Argyriou, C.-K. Loong, L. Christensen, J. Power Sources 68 (1997) 570.
[6] M.H. Rossouw, D.C. Liles, M.M. Thackeray, Prog. Batt. Batt. Mater. 15 (1996) 8.
[7] Q. Feng, H. Kanoh, Y. Miyai, K. Ooi, Chem. Mater. 7 (1995) 148.
[8] P.M. De Wolff, Acta Crystallogr. 12 (1959) 341.
[9] Y. Chabre, J. Pannetier, Prog. Solid State Chem. 23 (1995) 1.
[10] S. Sarciaux, A. Le Gal La Salle, A. Verbaere, Y. Piffard, D. Guyomard, Mater. Res. Soc. Symp. Proc. 548 (1999) 251.
[11] L.I. Hill, A. Verbaere, D. Guyomard, J. Electrochem. Soc., in press.
[12] K.-S. Han, P. Krtil, M. Yoshimura, J. Mater. Chem. 8 (1998) 2043.
[13] K.-S. Han, S. Tsurimoto, M. Yoshimura, Solid State Ionics 121 (1999) 229.
[14] E. Deltombe, N. de Zoubov, M. Pourbaix, Rapport technique du CEBELCOR, Gauthier, Villars and Cie, Paris, 1963.
[15] L.I. Hill, R. Portal, A. Le Gal La Salle, A. Verbaere, D. Guyomard, Electrochem. Solid-State Lett. 4 (2001) D1.
[16] L.I. Hill, R. Portal, A. Verbaere, D. Guyomard, Electrochem. Solid-State Lett. 4 (2001) A180.
[17] S. Sarciaux, Ph.D. Thesis, Université de Nantes, Nantes, France, 1998.
[18] C.S. Johnson, M.F. Mansuetto, M.M. Thackeray, Y. Shao-Horn, S.A. Hackney, J. Electrochem. Soc. 144 (1997) 2279.
[19] L.I. Hill, H. Arrivé, D. Guyomard, Ionics 8 (2002) 161.
[20] S. Sarciaux, A. Le Gal La Salle, A. Verbaere, Y. Piffard, D. Guyomard, J. Power Sources 81/82 (1999) 661.
[21] S. Sarciaux, A. Le Gal La Salle, A. Verbaere, Y. Piffard, D. Guyomard, J. Power Sources 81/82 (1999) 656.
[22] Q. Feng, H. Kanoh, K. Ooi, M. Tani, Y. Nakacho, Electrochem. Soc. Lett. 141 (1994) L135.
[23] J. Dai, S.F.Y. Li, K.S. Siow, Z. Gao, Electrochim. Acta 45 (2000) 2211.